OPEN

Citation: Cell Death and Disease (2014) 5, e1270; doi:10.1038/cddis.2014.200

www.nature.com/cddis

Involvement of p38 in signal switching from autophagy to apoptosis via the PERK/eIF2α/ATF4 axis in selenite-treated NB4 cells

Q Jiang[1], F Li[1], K Shi[1], P Wu[1], J An[1], Y Yang[1] and C Xu*[,1]

Selenite has emerged as an optional chemotherapeutic agent for hematological malignancies. Autophagy and apoptosis are both engaged in selenite-induced cell death. In a previous report, we have identified heat shock protein 90 (Hsp90) as a critical modulator of the balance between autophagy and apoptosis in selenite-treated leukemia cells. However, the mechanisms by which selenite mediates the crosstalk between autophagy and apoptosis remain largely unknown. Herein, we demonstrate that the endoplasmic reticulum (ER) stress-related PERK/eIF2α/ATF4 pathway and p38 are core modules for the selenite-induced switch to apoptosis from autophagy. We found that selenite activated PERK and eIF2α/ATF4 downstream to promote apoptosis. During this progression, p38 was dissociated from PERK-inhibiting Hsp90 and became autophosphorylated. Then, activated p38 further enhanced the docking of activating transcription factor 4 (ATF4) onto the *CHOP* (CCAAT/enhancer-binding protein homologous protein) promoter via eIF2α to enhance apoptosis. We also found that activated p38 suppressed the phosphorylation of eIF4E that directed ATF4 to bind to the *MAP1LC3B* (*microtubule-associated protein 1 light chain 3B*) promoter. Because of the deactivation of eIF4E, the association of ATF4 with the *MAP1LC3B* promoter was inhibited, and autophagy was compromised. Intriguingly, p53 played important roles in mediating the p38-mediated regulation of eIF2α and eIF4E. When activated by p38, p53 induced the phosphorylation of eIF2α and the dephosphorylation of eIF4E, particularly in the nucleus where the ATF4 transcription factor was modulated, ultimately resulting in differential expression of CHOP and LC3. Moreover, selenite exhibited potent antitumor effects *in vivo*. In an NB4 cell xenograft model, selenite induced apoptosis and hampered autophagy. In addition, related signaling proteins demonstrated similar changes to those observed *in vitro*. These data suggest that selenite may be a candidate drug for leukemia therapy.

Cell Death and Disease (2014) **5,** e1270; doi:10.1038/cddis.2014.200; published online 29 May 2014
Subject Category: Cancer

Leukemia is a blood malignancy characterized by an abnormal increase in immature white blood cells.[1] Accumulating studies have shown that sodium selenite, representing a therapeutic option for leukemia, has the capacity to induce apoptosis in malignant cells. In addition, autophagy is believed to be involved in regulation of the programmed cell death induced by selenite sodium.

Autophagy, which degrades redundant or damaged cellular constituents, is considered a central component of the integrated stress response.[2] Decades of studies have demonstrated that autophagy and apoptosis may be interconnected and even simultaneously regulated by the same triggers in tumor cells.[3,4] Recent reports have shown that the antitumor activities of selenite are attributed to its capacity to evoke apoptosis by altering microtubule assembly[5] or change the autophagy level in tumor cells.[6,7] However, limited data are available with regard to the mechanisms regulating the crosstalk between apoptosis and autophagy in selenite-treated leukemia cells.[8]

As a major source and/or scaffold for autophagic membrane formation, the endoplasmic reticulum (ER) is crucial for autophagy elicitation under stress.[9] In response to ER stress, PKR-like ER kinase (PERK) and other protein kinases initiate the unfolded protein response (UPR) that is tightly related to the regulation of programmed cell death. Reports from Rouschop *et al.*[10] indicate that the UPR of the PERK/eIF2α/ATF4 pathway is a potent stimulator of autophagy.[11] In contrast, p38 mitogen-activated protein kinase (MAPK) is an essential effector mediating apoptosis or autophagy under ER stress.[12–14] We have discovered that p38 regulates autophagy, whereas the PERK/eIF2α/ATF4 pathway modulates apoptosis in selenite-treated leukemia cells.[7,15] However, the

[1]National Laboratory of Medical Molecular Biology, Institute of Basic Medical Sciences and School of Basic Medicine, Peking Union Medical College and Chinese Academy of Medical Sciences, Beijing, China
*Corresponding author: C Xu, Department of Biochemistry and Molecular Biology, Institute of Basic Medical Sciences, Chinese Academy of Medical Sciences (CAMS) and Peking Union Medical College (PUMC), 5 DongdanSantiao, Dongcheng District, Beijing 100005, China. Tel: +86 10 69156445; Fax: +86 10 69156445; E-mail: cmxu@ibms.pumc.edu.cn
Keywords: p38; selenite; autophagy; apoptosis; p53
Abbreviations: MAPK, mitogen-activated protein kinase; AML, acute myelogenous leukemia; APL, acute promyelocytic leukemia; ER, endoplasmic reticulum; ATF4, activating transcription factor 4; CHOP, CCAAT/enhancer-binding protein homologous protein; Hsp90, heat shock protein 90; eIF2α, eukaryotic translation initiation factor 2 subunit-α; eIF4E, eukaryotic translation initiation factor 4E; MAP1LC3B, microtubule-associated protein 1 light chain 3B; Mknk1, MAP kinase interacting serine/threonine kinase 1; s.c., subcutaneous
Received 09.12.13; revised 04.4.14; accepted 08.4.14; Edited by GM Fimia

detailed mechanisms underlying the crosstalk between apoptosis and autophagy remain largely unknown.

In this study, we found that the p38-associated PERK/eIF2α/ATF4 pathway dictates the switch from autophagy to apoptosis. Moreover, the antitumor activity of selenite was characterized *in vivo* using a leukemia cell line xenograft model, launching many new possibilities for human hematological malignancy therapy.

Results

p38 is critical for ATF4 upregulation in response to selenite-induced ER stress. Multiple stress responses, including apoptosis and autophagy, are integrated in the ER,[16,17] and ER stress may affect the balance among these responses. Therefore, we investigated the effects of selenite on ER stress-related signal pathways. The expression of p-PERK, p-eIF2α, ATF4 (activating transcription factor 4) and CHOP (CCAAT/enhancer-binding protein homologous protein) was gradually increased after selenite incubation (Figure 1a), indicating that selenite triggers ER stress. To confirm this result, NB4 cells were incubated with the ER stress inducer tunicamycin (Tm). Similarly, the PERK/eIF2α/ATF4 axis and CHOP upregulation were induced (Figure 1b), with both treatments inducing apoptosis in a time-dependent manner (Figures 1a and b), strengthening our hypothesis that selenite-induced ER stress is related to cell-fate regulation. Moreover, the transcription factor ATF4 was increased in both nuclear and cytoplasmic fractions after exposure to selenite (Figure 1c) that modulates the expression of various target genes to exert effects on stress responses.

Because p38 MAPK expression remained intact, selenite enhanced p38 phosphorylation in a time- and concentration-dependent manner (Figure 1d). Because MAPKs are implicated in the regulation of many cellular processes, we examined the impact of p38 on ATF4 expression. SB203580, a specific inhibitor of p38, strongly abrogated selenite-mediated ATF4 upregulation (Figure 1e). Hence, we hypothesized that p38 might play a critical role in selenite-induced ATF4 upregulation. To validate this hypothesis, siRNA and plasmid transfections were performed. As shown

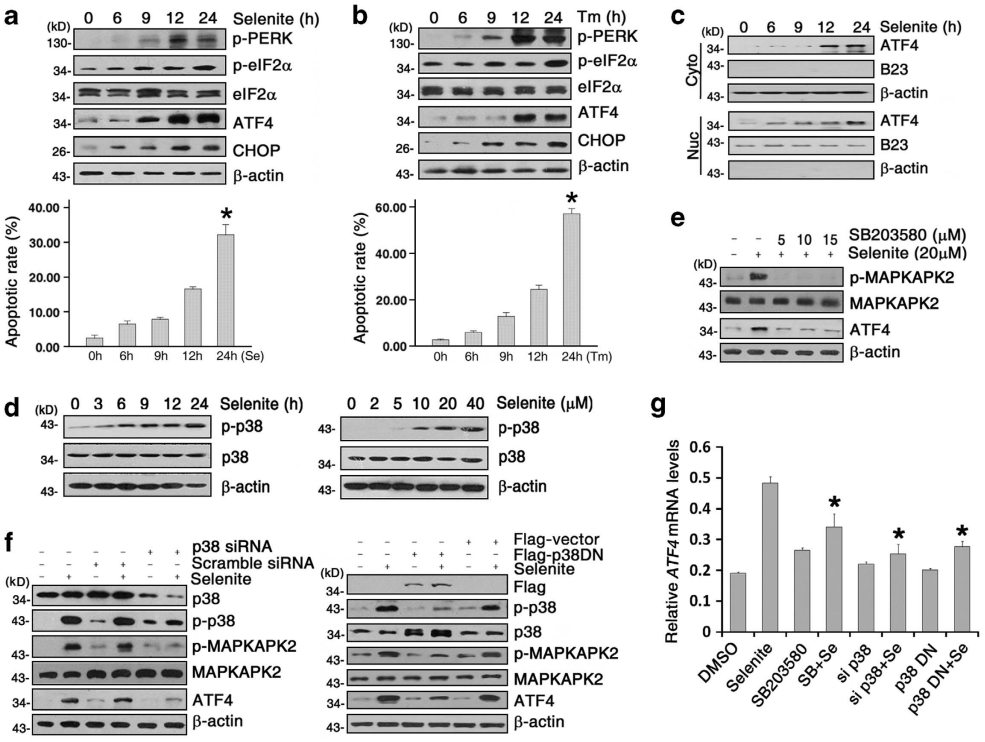

Figure 1 p38 upregulates ATF4 levels in response to selenite. (**a** and **b**) ER stress and apoptosis. Both selenite (**a**) and tunicamycin (**b**) induced the ER stress-related PERK/eIF2α/ATF4 pathway, downstream CHOP and finally apoptotic death. NB4 cells were treated with 20 μM selenite or 0.1 μg/ml tunicamycin, collected at various intervals and lysed, and the lysates were then subjected to western blot assay. In addition, cells were stained with Annexin-V and PI (lower panels), and apoptotic cells were counted with a cytometer. The data are presented as the means ± S.D. ($n = 3$). *$P < 0.05$ compared with the 0 h group. (**c**) ATF4 expression in the cytoplasm and nucleus. Cytoplasmic and nuclear fractions were isolated at indicated times, and ATF4 was examined by western blot analysis. β-Actin and B23 were used to confirm the purity of the cytoplasmic and nuclear fractions, respectively. (**d**) Selenite activates p38 in a time- and concentration-dependent manner. NB4 cells were treated with 20 μM selenite for various times (left panel) or with the indicated concentrations of selenite for 24 h (right panel), and p-p38 and p38 expression was then determined. (**e**) p38 is involved in ATF4 regulation. Cells were pretreated with 5, 10 or 15 μM of the p38-specific inhibitor SB203580 and then incubated with selenite for 24 h. p-MAPKAPK2, MAPKAPK2 and ATF4 were probed using western blot assay. (**f**) p38 suppression inhibited ATF4 expression. NB4 cells were transfected with siRNA targeting p38 (left panel) or a plasmid encoding dominant negative p38 (right panel), incubated with selenite for 24 h and the indicated proteins were then probed. (**g**) ATF4 expression was affected by p38 at the mRNA level. Before selenite exposure, cells were treated with SB203580, or they were transfected with p38-siRNA or the p38DN plasmid. ATF4 mRNA was also quantified by qRT-PCR. The blots are representative of at least three separate experiments. The data presented are representative of these results. The statistical graphs are presented as the means ± S.D. *$P < 0.05$ compared with selenite-treated cells

in Figures 1f and g, the interference of p38 phosphorylation resulting from siRNA-mediated p38 downregulation or dominant-negative p38 expression sharply hampered ATF4 expression in selenite-treated cells. Taken together, our data suggest that p38 is essential for the modulation of ER stress-related ATF4 upregulation in selenite-treated cells.

p38 modulates the switch from autophagy to apoptosis. Because p38 participated in the regulation of the ER stress signal, we subsequently determined the effects of p38 on cell fate. A CCK-8 assay showed that the p38 antagonist SB203580 protected NB4 cells from selenite insult (Figure 2a). Flow cytometric data further supported p38 inhibition, reducing the number of dead cells in selenite-treated groups (Figure 2b). A western blot assay also demonstrated that p38 inhibition blocked PARP and caspase 3 cleavage (Figure 2c), suggesting that p38 activation plays an important role in selenite-induced apoptosis. Conversely, loss of p38 resulted in autophagy enhancement. As shown in Figure 2c, the deactivation or depletion of p38 in selenite-treated cells induced Beclin1 expression, the conversion of LC3-I to LC3-II and decreased p62 expression. Next, we analyzed how p38 inhibition affects LC3 distribution and conversion in cells transfected with GFP-LC3 plasmids. The p38 inhibition caused a redistribution of LC3 from cytoplasmic diffusions to discrete vesicular structures (punctate fluorescence) and the upregulation of GFP-LC3-II protein in selenite-treated cells (Figures 2d and e). In addition, transmission electron microscopy (TEM) revealed that the number of autophagosomes, typically characterized by scattered double-membrane structures containing recognizable cellular organelles, was partially restored in cells preincubated with the p38 inhibitor (Figure 2f). These data illustrated that p38 negatively modulates autophagy in selenite-treated cells.

Because p38 exerts opposite effects on apoptosis and autophagy, we examined how cell fate was affected by the imbalance between these programmed death processes. Compared with bafilomycin A1 (Baf A1), another autophagy antagonist, 3-methyladenine (3-MA), showed higher inhibition efficacy in NB4 cells (Figure 2g) and were used in subsequent tests. NB4 cells were treated with selenite in the presence of 3-MA and SB203580 alone or simultaneously, and apoptotic markers were examined. As shown in Figure 2h and Supplementary Figure S1, 3-MA augmented selenite-induced apoptosis that was partially reversed by SB203580 treatment. These results indicated that p38 activation switches the cell fate from apoptotic death to protective autophagy in selenite-treated cells.

PERK-mediated p38 activation transduces signals to eIF2α, thereby regulating ATF4 expression. To gain further insight into the mechanisms by which p38 regulates apoptosis and autophagy, we explored the interaction between p38 and the PERK/eIF2α/ATF4 pathway. When p38 was inhibited or depleted, the expression of p-eIF2α and ATF4 was significantly hampered, whereas upstream p-PERK was only slightly affected (Figure 3a). PERK silencing via siRNA suppressed the phosphorylation but not expression of p38 (Figure 3b). Moreover, we tested the effects of eIF2α (eukaryotic translation initiation factor 2 subunit-α) on p38 activity. Salubrinal, a cell-permeable eIF2α agonist,[18] effectively activated eIF2α at 5 μM in NB4 cells (Figure 3c). However, salubrinal treatment exerted limited effects on p38 phosphorylation when ATF4 expression was highly increased (Figure 3d). Consistent with these results, the expression of ATF4 was weakened by eIF2α-siRNA transfection when the p38 signal was unchanged (Figure 3b). These results demonstrated that p38 acts between PERK and eIF2α to promote signal transduction to ATF4.

p38 colocalized with Hsp90 in NB4 cells. MAPK kinase 3 (MKK3) and MKK6 are commonly regarded as the upstream p38 activators in response to cellular stress and cytokines.[19] Surprisingly, various doses or intervals of selenite treatment have failed to alter the phosphorylation of MKK3/6 (Figure 3e), indicating that selenite-induced p38 activation is independent of MKK3/6. Because dissociation from heat shock protein 90 (Hsp90) evokes p38 activation in an autophosphorylation manner,[20] the interaction between p38 and Hsp90 was examined. Co-IP and GST pull-down assays showed that p38 bound to Hsp90, and this physical approximation was inhibited by selenite (Figures 3f and g). Immunofluorescence microscopy provided more direct evidence that selenite blocked the colocalization of p38 with Hsp90 (Figure 3h).

PERK-mediated Hsp90 inhibition promotes the activation of p38. We performed subsequent experiments to examine the potential interaction between Hsp90 and p38. Cotreatment with the Hsp90-specific inhibitor 17-AAG and selenite increased apoptosis and decreased the viability of NB4 cells (Figures 4a–c), indicating a protective role for Hsp90 in selenite-induced apoptosis. Hsp90 overexpression greatly inhibited the selenite-induced upregulation of p-p38 and ATF4, whereas Hsp90 depletion or inhibition increased the expression of these proteins (Figure 4d). We therefore speculated that Hsp90 release of p38 is an important signal for selenite-induced apoptosis. To determine the relationship between Hsp90 and the PERK pathway, we detected the expression of Hsp90 in PERK-siRNA-transfected cells. Consistent with a previous report,[21] selenite-induced Hsp90 downregulation was reversed with inhibition of PERK expression (Figure 4e). Moreover, co-IP and immunofluorescence demonstrated that a direct interaction exists between PERK and Hsp90 (Figures 4f and g). Taken together, it is reasonable to deduce that Hsp90 bridges the gap between p38 and the PERK/eIF2α/ATF4 axis.

ATF4 binds the *MAP1LC3B* and *CHOP* promoters. Given that ATF4 binds to a cAMP-responsive element (CRE: 5′-TGACCTCA-3′) to initiate the expression of autophagy-related genes,[10,22,23] we investigated whether ATF4 directly transactivated *MAP1LC3B* (*microtubule-associated protein 1 light chain 3B*) in NB4 cells. Computational analysis identified two putative CRE-like elements, spanning −528 to −340 (a) and −1895 to −1723 (A) in the *MAP1LC3B* promoter. *CHOP*, a known target of ATF4, also has those *cis*-acting elements (site b and site B) in its promoter (Figure 5a). ChIP assays demonstrated that ATF4 indeed bound to the

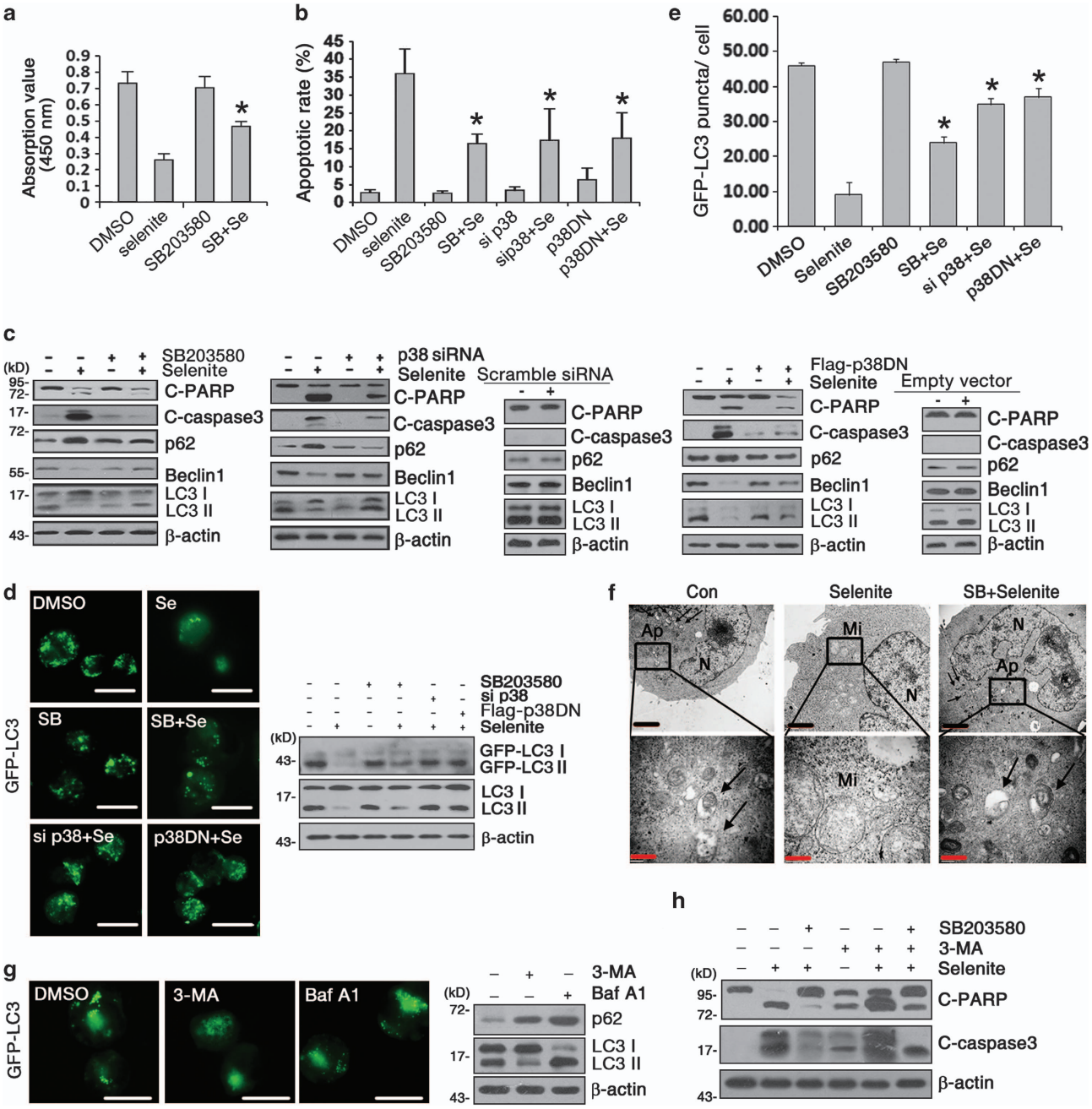

Figure 2 Effects of p38 on selenite-modulated apoptosis and autophagy in NB4 cells. (**a**) The viability of cells treated with selenite in the presence or absence of SB203580 was analyzed using the CCK-8 kit. (**b**) p38 inhibition relieved selenite-induced apoptosis. NB4 cells were preincubated with SB203580, and selenite-induced apoptosis was then examined using flow cytometry. (**c**) p38 signaling negatively regulates autophagy. Before selenite treatment, p38 was deactivated with a specific antagonist, siRNA or DN plasmid. After 24 h, markers related to apoptosis and autophagy were separately probed. (**d**) p38 effects on LC3 conversion. p38 was suppressed in NB4 cells transiently expressing GFP-LC3. GFP-LC3 puncta (left panel) and conversion to GFP-LC II (right panel) were also examined using immunofluorescence microscopy and western blot assay. Scale bar, 20 μm. (**e**) The average number of GFP-LC3 puncta per cell. For each data point, the mean number in 30 cells from 4 independent experiments was calculated. (**f**) Electron micrograph of NB4 cells incubated with selenite in the presence or absence of SB203580. Black arrows indicate autophagosomes. N, nucleus; Mi, mitochondria; Ap, autophagosome. Bar, 2 μm (upper panels); 0.4 μm (bottom panels). (**g**) Punctate GFP-LC3 fluorescence (left panel) and the expression of p62 and LC3 (right panel) in GFP-LC3 plasmid-transfected cells treated with DMSO, 3-MA (10 mM) or Baf A1 (100 μM). Bar, 20 μm. (**h**) Cells were incubated with SB203580 and 3-MA alone or in combination, and the c-PARP and c-caspase3 levels were then determined by western blot assay. The blots are representative of at least three separate experiments. The data are presented as the means ± S.D. $^*P < 0.05$ compared with selenite-treated cells

cis-acting elements within the *MAP1LC3B* and *CHOP* promoters in NB4 cells (Figure 5b). It is noteworthy that the increase in the amount of enriched ATF4 on the *CHOP* promoter resulting from selenite treatment was relieved by p38 inhibition, in contrast to the reduced amounts that were recovered from the *MAP1LC3B* promoter (Figure 5b).

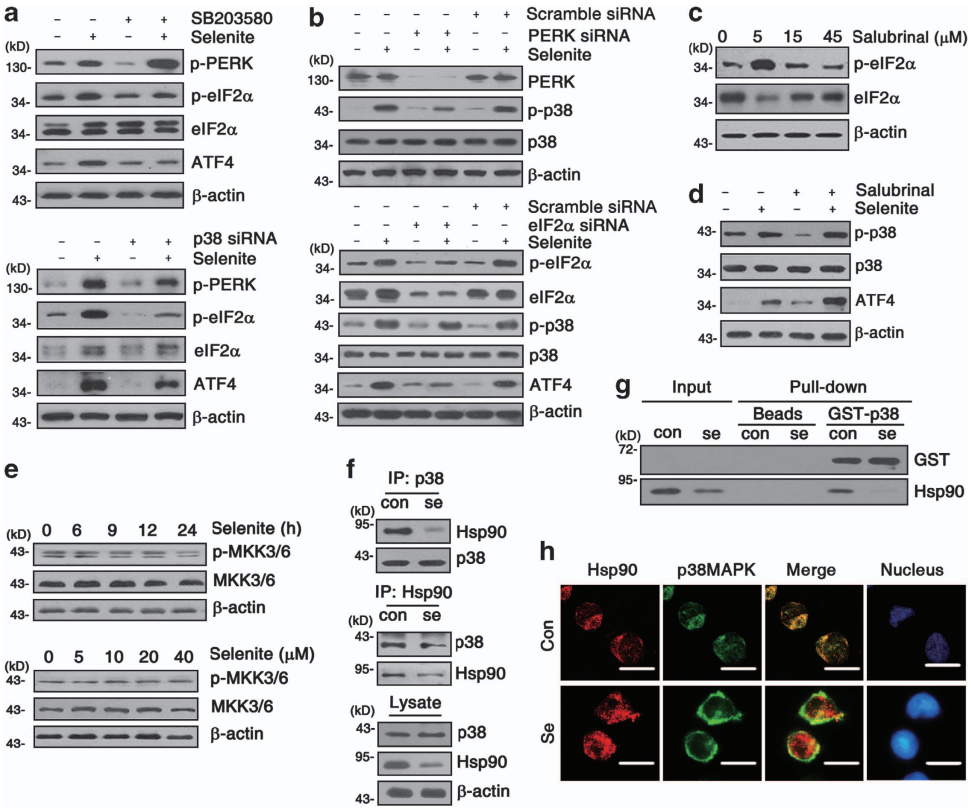

Figure 3 p38-mediated eIF2α phosphorylation transduces signals from PERK to ATF4. (**a**) p38 was inhibited with SB203580 (upper panel) or p38-siRNA (lower panel), and the cells were then treated with selenite for 24 h. Total lysates were extracted, and p-PERK, p-eIF2α, eIF2α and ATF4 were probed using a western blot assay. (**b**) Following PERK (upper panel) or eIF2α (lower panel) inhibition and subsequent selenite exposure, the expression of proteins of interest were examined. (**c**) Cells were treated with the indicated concentrations of salubrinal, and p-eIF2α and eIF2α were probed. (**d**) Cells were treated with 5 μM salubrinal alone or in combination with selenite. Proteins of interest were detected using western blot analysis. (**e**) Cells were incubated with 20 μM selenite for various times or the indicated concentrations of selenite for 24 h, and the expression of p-MKK3/6 and MKK3/6 were then examined. (**f**) Cells treated with or without selenite were lysed, and total lysates were incubated with anti-p38 or anti-Hsp90 antibodies and then coincubated with protein A + G beads. After washing, the proteins bound to beads were eluted and subjected to a western blot assay. (**g**) Total lysates were coincubated with GST-p38 and GSH beads and rinsed. The proteins bound to GSH beads were eluted and blotted after PAGE electrophoresis. The blots are representative of at least three separate experiments. (**h**) Cells were fixed on slides, blocked and sequentially stained with primary antibodies and secondary antibodies. Images were then recorded using an immunofluorescence microscope. Nuclei were stained with DAPI. Bar, 20 μm. Data are representative of at least three separate experiments

In addition, a qRT-PCR assay showed that p38 suppression significantly reversed selenite-upregulated *CHOP* expression at the mRNA level (Figure 5c). At the protein level, p38 deactivation or deletion led to decreased CHOP expression and enhanced LC3-II expression (Figure 5d). Together with the above-mentioned data, p38 is suggested to direct a preferential association between ATF4 and the *CHOP* promoter under stress, thus promoting apoptosis and suppressing autophagy.

Signal modules downstream of p38 determine ATF4 substrate specificity. To explore how the ATF4 substrate specificity is determined, we examined the eIF4E (eukaryotic translation initiation factor 4E) signal that was reported to act downstream of p38 to regulate ATF4.[24] Selenite treatment resulted in a moderate increase in the phosphorylation levels of eIF2α but a dramatic decline in eIF4E phosphorylation (Figure 6a). Subsequently, discrepancies in the changes between p-eIF2α and p-eIF4E were observed in the nucleus, where the ATF4 transcription factor is regulated. As shown in Figure 6b, the nuclear accumulation of p-eIF2α was enhanced by selenite, whereas p-eIF4E was reduced in the nucleus. These results suggest the possibility that eIF2α and eIF4E are mediated by the substrate selection of ATF4 under selenite treatment. To test this hypothesis, we used salubrinal and the Mknk1 (MAP kinase interacting serine/threonine kinase 1) inhibitor to inspect the roles of eIF2α and eIF4E in apoptosis- and autophagy-related protein expressions. Salubrinal pretreatment upregulated eIF2α phosphorylation and CHOP expression and suppressed LC3 conversion (Figure 6c). When eIF4E was inhibited, LC3 conversion was reduced, but CHOP expression was slightly affected (Figure 6c). Additional experiments confirmed that CHOP expression and LC3 conversion were mainly regulated by eIF2α and eIF4E, respectively (Figure 6c). A ChIP assay demonstrated that alterations in eIF2α were biased toward affecting the binding efficiency of ATF4 to the *CHOP* promoter in selenite-treated cells compared with that of eIF4E that mainly regulates the association between ATF4 and the *MAP1LC3B* promoter (Figure 6d). Furthermore, qRT-PCR and immunofluorescence assays confirmed that the association between ATF4

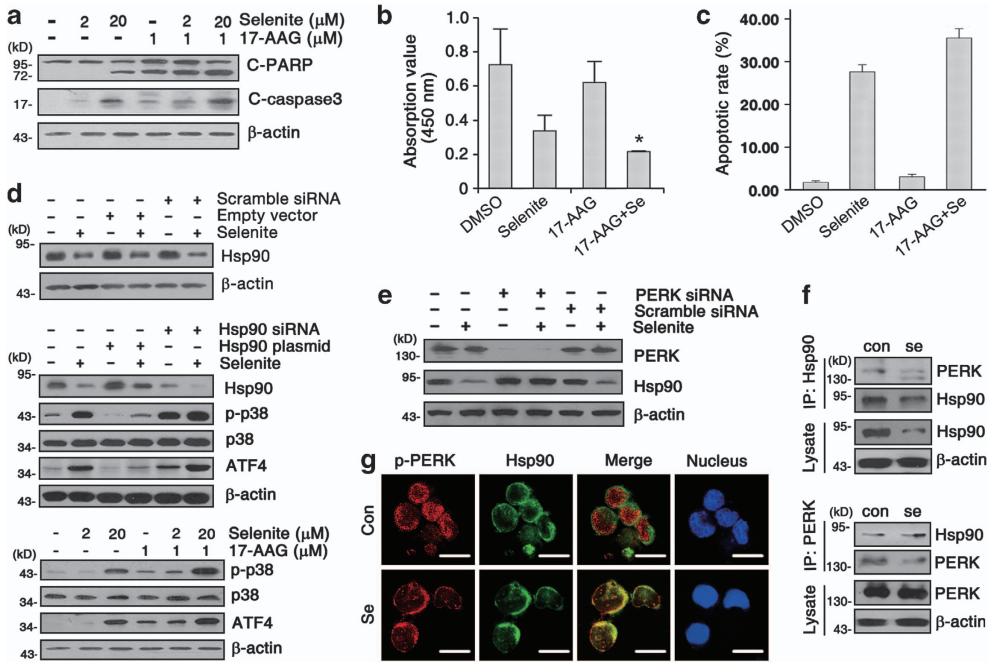

Figure 4 PERK negatively regulates p38 activity via Hsp90. (**a**) Cells were cotreated with the Hsp90 inhibitor 17-AAG and the indicated concentrations of selenite for 24 h. Cell lysates were then subjected to western blot assays to determine c-PARP and c-caspase 3 expression. (**b** and (**c**) Following 17-AAG and 20 μM selenite cotreatment, cell viability and apoptosis were assessed using the CCK-8 kit (**b**) or Annexin V/PI staining kit (**c**). *$P<0.05$ compared with selenite-treated cells. (**d**) The effects of Hsp90 on p38. Cells were treated with 20 μM selenite after transfection with PERK-siRNA, scrambled siRNA (upper panel) or with the indicated concentrations of selenite after 17-AAG incubation (lower panel). Then, the cells were lysed and subjected to western blot assay. The proteins of interest were blotted. (**e**) Cells were transfected with PERK-specific or scrambled siRNA, and the indicated proteins were probed after selenite incubation. (**f**) The physical interaction between Hsp90 and PERK was examined using co-IP. (**g**) Colocalization of p-PERK (red) and Hsp90 (green) was visualized by immunofluorescence microscopy. Nuclei were stained with DAPI. Bar, 20 μm. The blots are representative of at least three separate experiments. All experiments were conducted three times

and the *CHOP* or *MAP1LC3B* promoters was separately regulated by eIF2α and eIF4E. As shown in Figure 6e, CHOP expression was affected by the eIF2α activity change but not that of eIF4E. With regard to LC3 conversion, eIF4E exerted more obvious effects than eIF2α (Figures 6f and g). These findings indicated that the selenite-induced differential regulation of eIF2α and eIF4E leads to a discrepancy in the association between *CHOP* and *MAP1LC3B* and ATF4.

p38-mediated eIF2α phosphorylation depends on the p53 activity in response to selenite. p38 is tightly related to the regulation of p53 activity,[25] and we have demonstrated that wild-type p53 is essential for the NB4 cell response to selenite.[26] Herein, we asked whether p53 was involved in p38-meditated signal transduction. In selenite-treated cells, we found that p53 phosphorylation was upregulated in the cytoplasm and nucleus (Figure 7a). Then, we surveyed the interaction between p38 and p53. Co-IP and immunofluorescence microscopy demonstrated that selenite strengthened the molecular binding between p38 and p53 (Figure 7b and Supplementary Figure S2). As we inhibited or depleted p38, the activation of p53 was significantly suppressed (Figure 7c), indicating that p38 positively regulates p53 activity in NB4 cells. To test how this interaction was connected to the p38-meditated switch between autophagy and apoptosis, we tested the effects of p53 on cell death. As presented in Figures 7d and e, LC3-II expression and autophagosome formation were promoted after selenite treatment when p53 was deactivated in cells transfected with a plasmid encoding a mutant p53 (p53MT). However, apoptosis-related CHOP was severely downregulated by p53 inhibition. Moreover, a ChIP assay depicted that p53 was involved in the transcriptional regulation of *CHOP* and *MAP1LC3B*. p53 suppression interfered with ATF4 binding to the *CHOP* promoter and led to decreased amounts of CHOP mRNA in selenite-treated cells (Figure 7f). Conversely, p53 deactivation almost eliminated the selenite-induced dissociation of ATF4 from the *MAP1LC3B* promoter (Figure 7f). Therefore, we further surveyed the effects of p53 on eIF2α and eIF4E. p53 suppression simultaneously relieved the hyperactivation of eIF2α and deactivation of eIF4E in the cytoplasm and nucleus of selenite-treated cells (Figure 7g). These data established the core position of p53 in transducing the p38 signal to downstream cascades, including eIF2α and eIF4E, and eventually contributing to a selenite-driven switch from autophagy to apoptosis.

Sodium selenite suppresses tumor growth and autophagy *in vivo*. To investigate the antitumor effects of selenite *in vivo*, xenograft models of leukemia NB4 cells were established as described in the Materials and Methods. As shown in Figure 8a, selenite inhibited tumor growth in a dose-dependent manner. At 3 weeks after injection, the low selenite dose suppressed tumor growth, whereas

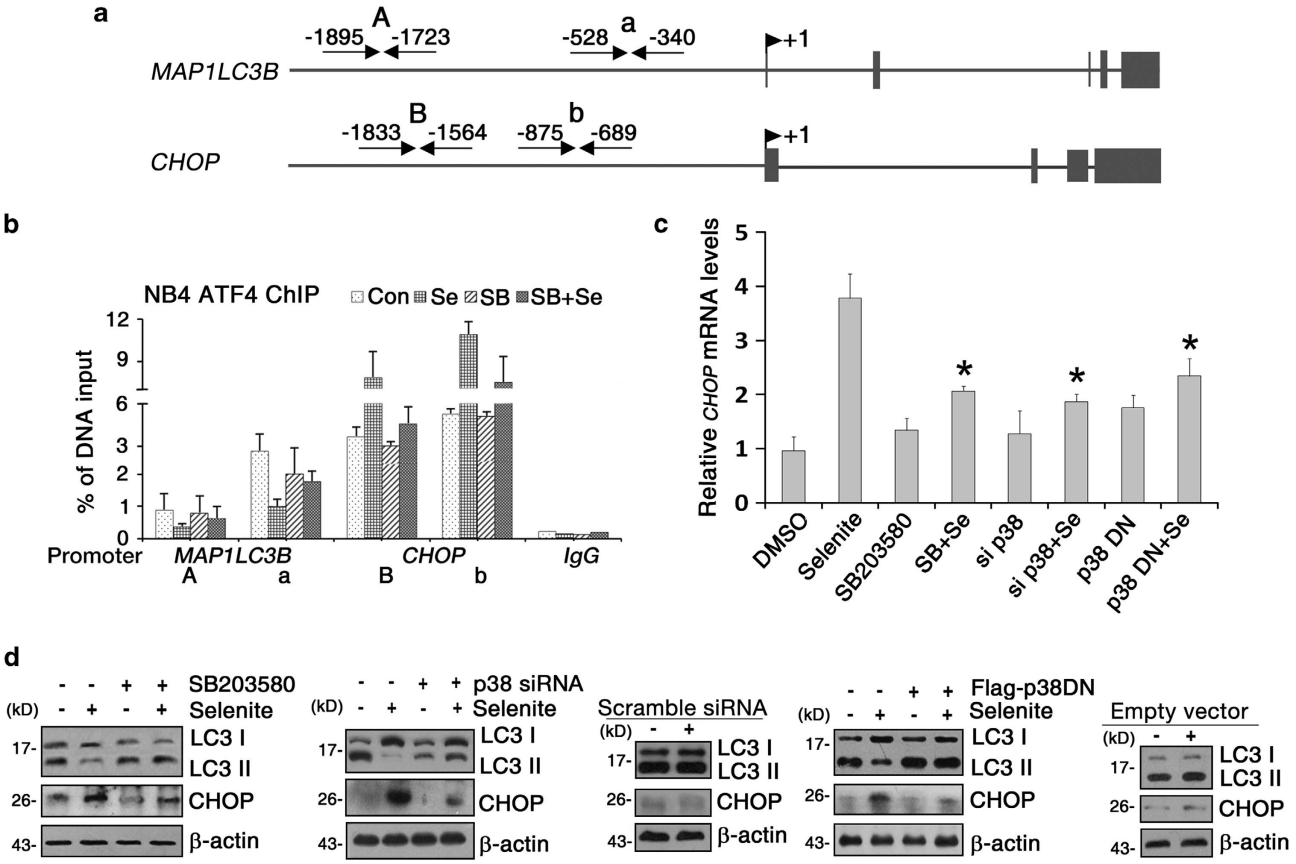

Figure 5 ATF4 is involved in *MAP1LC3B* and *CHOP* transcriptional regulation. (**a**) A schematic diagram showing the location of the sequences detected by quantitative PCR (qPCR) analysis following ChIP experiments. (A and a) two putative ATF4-binding CRE sites in the *MAP1LC3B* promoter; (B and b): two putative ATF4-binding CRE sites in the *CHOP* promoter. (**b**) Relative quantity of the *MAP1LC3B* and *CHOP* gene promoters occupied by ATF4. Cells were cotreated with SB203580 and selenite, and a ChIP assay was performed using an anti-ATF4 antibody and negative control IgG. The precipitated DNA was then assessed using qPCR analysis. (**c**) Cells were treated as indicated, and total mRNA was extracted. *CHOP* mRNA was quantified by qRT-PCR and normalized to DMSO-treated cells. (**d**) p38 regulates LC3 conversion and *CHOP* expression. After p38 was compromised via the indicated ways, cells were lysed, lysates were subjected to western blot assay, and LC3 conversion and CHOP expression were determined. The blots are representative of at least three separate experiments. The statistical graphs are presented as the means ± S.D. of three independent experiments. $^*P < 0.05$ compared with selenite-treated cells

the high dose more vigorously decreased the tumor volume. To determine whether selenite-induced tumor growth inhibition was related to apoptosis, tumor tissues were investigated using histopathological and TUNEL staining. In selenite-treated xenografts, nuclear condensation occurred (Figure 8b). Because nuclear condensation is an indicator of apoptosis, a TUNEL assay was performed. As expected, extensive DNA fragmentation was observed in selenite-treated tissues (Figure 8b), indicating that selenite induces NB4 cell apoptosis *in vivo*. Moreover, the expression of caspase 3, autophagy-associated LC3B and p62 were altered in selenite-treated tumors. IHC assays showed that the LC3B protein was decreased, whereas p62 and caspase 3 were upregulated in selenite-treated cells (Figure 8c), suggesting that selenite induces apoptosis and downregulates autophagy *in vivo*. To verify these results, tumor tissues were further analyzed by western blot. Consistent with the above observations, selenite induced apoptosis while decreasing autophagy in xenograft tumor cells (Figure 8d). In addition, we investigated alterations in key signaling molecules *in vivo*. As observed in our cell model, p-p38, p-p53, and AFT4 were strongly upregulated, whereas Hsp90 sharply decreased in the mouse model (Figures 8d and e).

Discussion

Traditional chemotherapy for acute myelogenous leukemia (AML) aims to induce the apoptosis of malignant cells.[27,28] Nevertheless, chemotherapeutic drugs lead to autophagy as well. Recently, several lines of evidence have pointed to the existence of an interconnection between apoptosis and autophagy. As autophagy may antagonize apoptosis, a critical issue becomes clarifying the mechanisms of antitumor drug action.[11,14] Here, we defined the involvement of a molecular switch, p38, in apoptosis and autophagy in selenite-treated human leukemia NB4 cells, schematically summarized in Figure 8f.

In addition to a signaling pathway related to ER stress-induced apoptosis, the PERK/eIF2α/ATF4 UPR branch is linked to autophagy in various diseases.[29,30] Herein, we observed that PERK modulates p38 phosphorylation that affects the target selection of ATF4 to mediate the switch between autophagy and apoptosis. Thus, p38 is a critical

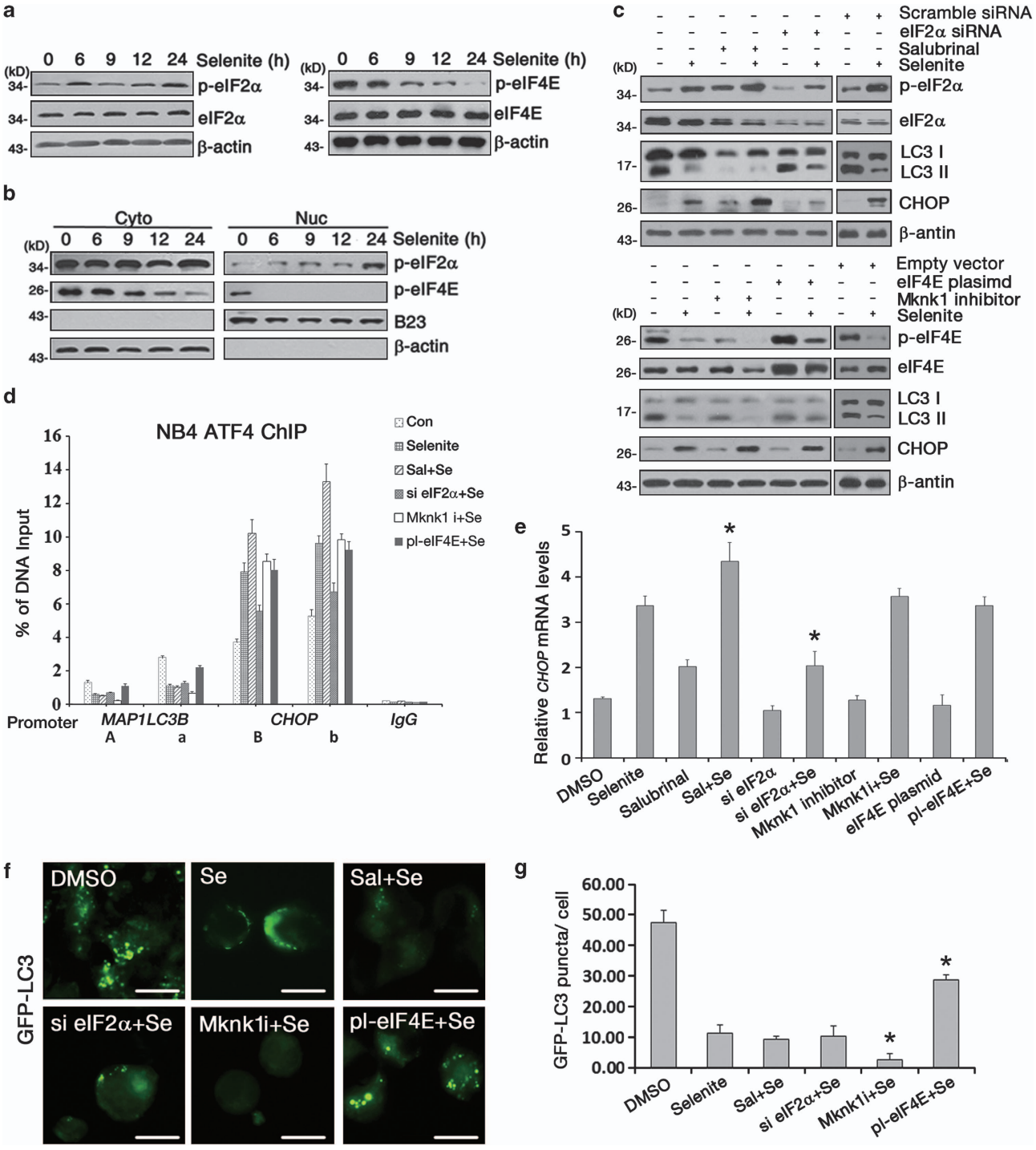

Figure 6 ATF4 promoter selection depends on the p38-mediated phosphorylation eIF4E or eIF2α. (**a** and **b**) At the indicated intervals of selenite treatment, p-eIF2α, eIF2α, p-eIF4E and eIF4E expression was examined in whole cell lysates (**a**) or in cytoplasmic and nuclear fractions (**b**) using the western blotting assay. (**c**) Effects of eIF2α and eIF4E on cell death. (Upper panel) Cells were treated with the eIF2α activator salubrinal or transfected with eIF2α-siRNA and then incubated with selenite. (Lower panel) Cells were treated with the inhibitor Mknk1 (1 μM) or transfected with an eIF4E plasmid before selenite treatment. The indicated proteins were probed using western blot. (**d**) Relative quantitative analysis of the promoters of the *MAP1LC3B* and *CHOP* genes occupied by ATF4 under the conditions indicated. (**e**) *CHOP* mRNA was quantified by qRT-PCR. (**f**) Punctate GFP-LC3 fluorescence in GFP-LC3-transfected cells treated with various chemicals. Bar, 20 μm. (**g**) The average number of GFP-LC3 puncta per cell. Each data point represents a mean count of GFP-LC3 puncta in 30 cells from independent experiments. The blots are representative of at least three separate experiments. The data are presented as the means ± S.D. $^*P < 0.05$ compared with selenite-treated cells

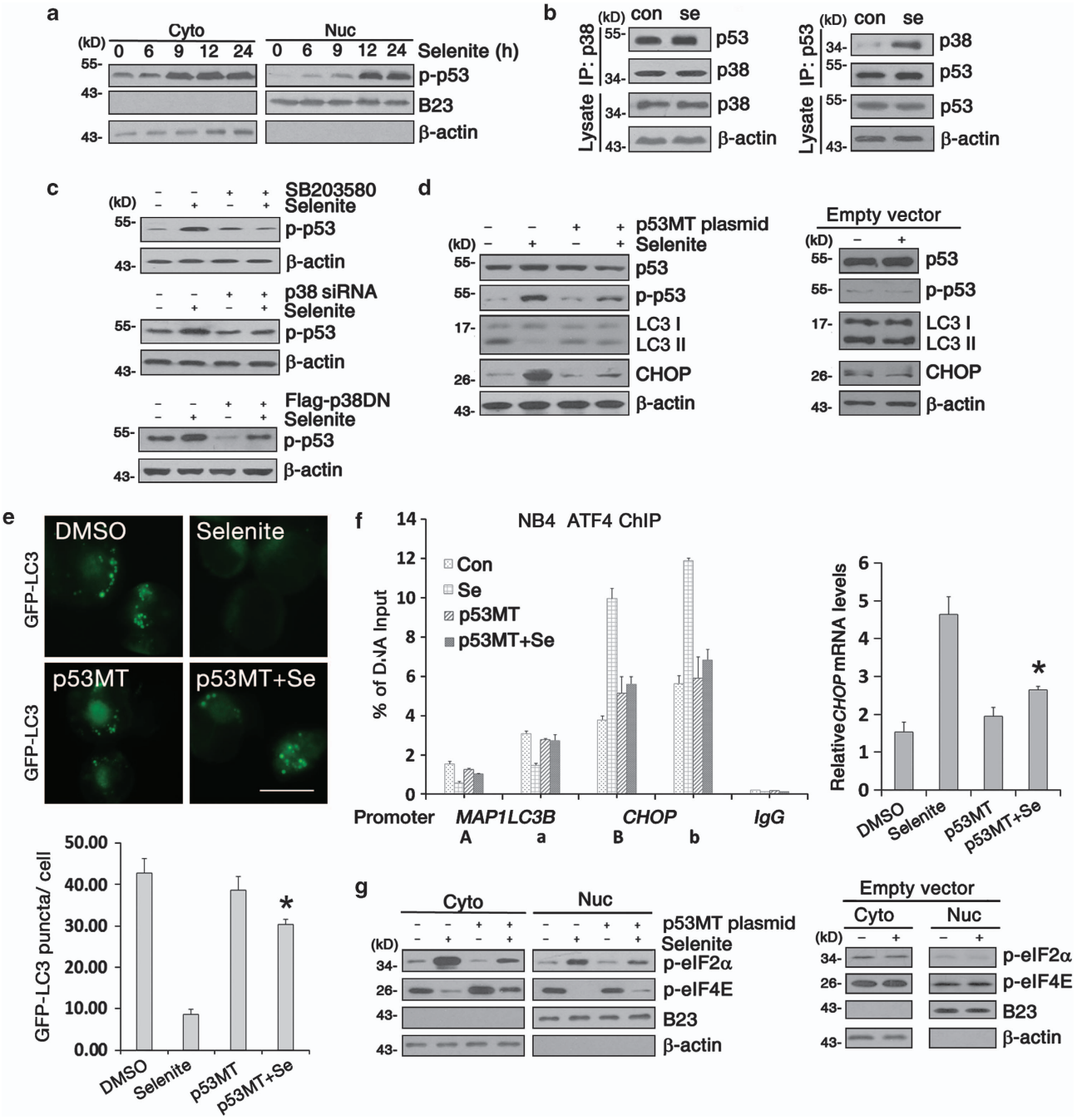

Figure 7 p53 serves as a key regulator of the p38 targets. (**a**) Cellular distribution of p-p53 in NB4 cells after selenite treatment for the indicated durations. (**b**) Co-IP of p53 and p38. (**c**) p38 was inhibited as indicated, and p-p53 was probed. (**d**) NB4 cells were transfected with the p53MT plasmid before selenite treatment, and the expression of p53, p-p53, LC3 and CHOP were then analyzed by western blot assay. (**e**) Following co-transfection with the GFP-LC3 and p53MT plasmids, cells were treated with selenite. The fluorescence signal was then captured using a microscope (upper), and GFP puncta were calculated (lower). Bar, 20 μm. (**f**) Relative quantitative analysis of the *MAP1LC3B* and *CHOP* promoters occupied by ATF4 under the indicated conditions (left panel). The data are expressed as the percentage of input DNA. *CHOP* mRNA was quantified by qRT-PCR (right panel). (**g**) Western blots analysis of p-eIF2α and p-eIF4E in different compartments of cells transfected with the p53MT plasmid. The blots are representative of at least three separate experiments. The data are presented as the means ± S.D. of at least three independent experiments. *$P<0.05$ compared with selenite-treated cells

factor linking the PERK/eIF2α/ATF4 cascade to apoptosis and autophagy crosstalk.

p38 is believed to regulate both apoptosis and autophagy. Our data indicated that autophosphorylation at Thr^{180}/Tyr^{182} and the resulting activation of p38 is an important event in selenite-induced cell death *in vitro* and *in vivo*. Our observation that p38 suppressed autophagy but promoted apoptosis in response to selenite is partially consistent with the report of Keil *et al*.[31] However, there are studies indicating a reverse correlation between p38 and autophagy,[32,33] suggesting that

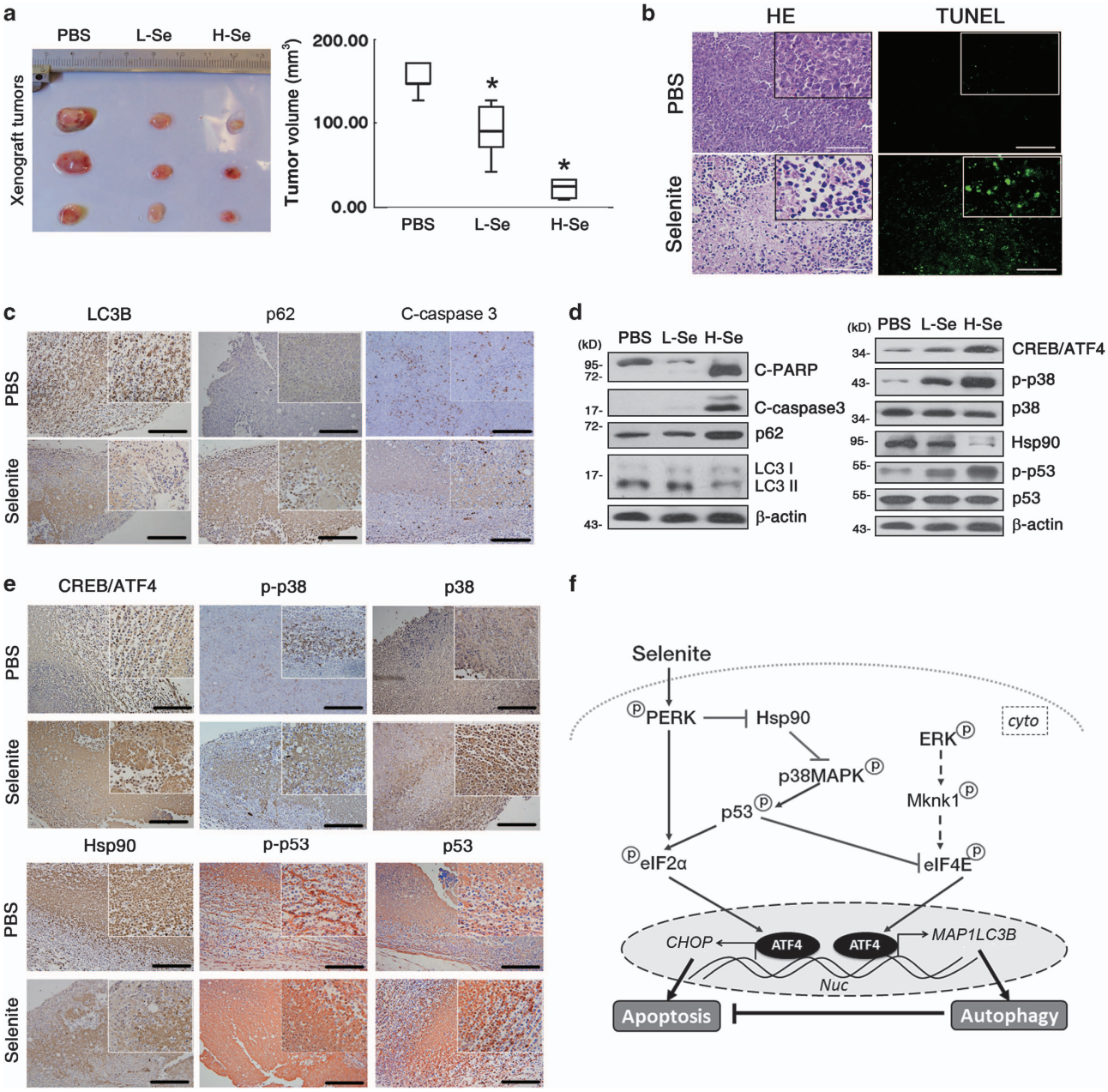

Figure 8 Selenite induced apoptosis and suppressed autophagy *in vivo*. (**a**) Representative tumors from NB4 cell xenograft mice and the tumor volume calculation (PBS, PBS treatment; L-Se, 3 mg/kg selenite every 2 days; H-Se, 6 mg/kg selenite every 2 days). $n = 7$. (**b**) Histopathological analysis and TUNEL staining of tumor tissues from PBS- and L-Se-treated-mice. (**c** and **e**) IHC analysis of xenografts from PBS- and L-Se-treated-mice. Fixed tumor samples were stained with the indicated antibodies and observed under a microscope. (**d**) Expression of the proteins of interest *in vivo*. Tumors were pooled and lysed and then subjected to western blot analysis. The indicated proteins were probed. (**f**) A schematic diagram illustrating the signaling pathways employed by selenite to induce cell death. The blots are representative of at least three separate experiments. The data are shown as the means ± S.D. *$P < 0.05$ compared with PBS-treated mice

p38 is either an inducer or inhibitor of autophagy depending on stimulus type.

One reason for the complexity of p38 signaling is the abundance of p38 activators. We unexpectedly found that p38 was activated by Hsp90, a noncanonical activator, instead of the typical MKK3/6 axis activated under stress conditions. Hsp90 is a highly conserved molecular chaperone that facilitates the maturation of numerous proteins including the ER-residing transmembrane protein kinases PERK and IRE1α.[33,34] In turn, Hsp90 expression is affected by PERK activity.[34,35] In addition, the Hsp90–Cdc37 chaperone complex was reported to suppress the autophosphorylation of p38, acting as a specific regulator of the p38 pathway.[20] In agreement with these studies, our data demonstrated that PERK activation by selenite decreased Hsp90 expression and subsequently led to p38 autophosphorylation.

Transcriptional control is an important strategy for p38 in regulating cell functions and processes.[36,37] Here, we showed

that p38 affected the expression of the apoptosis-related *CHOP* and autophagy-associated *MAP1LC3B* genes. Once activated, p38 distinctly affected downstream eIF2α and eIF4E in selenite-treated cells and then affected the association between the ATF4 transcription factor and the promoters of different genes. As the docking sequence for ATF4, CRE-like elements exist in the *CHOP* and *MAP1LC3B* promoters. However, ATF4 was inclined to bind the *CHOP* promoter rather than that of *MAP1LC3B* after selenite treatment because of a p38-mediated upregulation of p-eIF2α and downregulation of p-eIF4E. Through the differential modulations of eIF2α and eIF4E, p38 influences the transcription of key proteins and the switch from autophagy to apoptosis.

Intriguingly, p53 is involved in p38-mediated ATF4 regulation as well. p53 is well known for its proapoptotic effects and promotes selenite-induced apoptosis.[26] With regard to autophagy, p53 functions as a promoter or suppressor according to its subcellular distribution and target effectors.[38,39] In response to selenite, p53 distinctly regulates the activities of eIF2α and eIF4E to affect ATF4 binding to the promoters of target genes. Finally, p53 upregulated CHOP to promote apoptosis, and it inhibited LC3 conversion to suppress autophagy. Together with our data in p53-deficient Jurkat cells in which selenite induced marked autophagic responses, it is suggested that p53 is of great importance for the balance between apoptosis and autophagy.[7] In fact, Zhu *et al.*[40] reported that p53 is the key modulator connecting apoptosis to autophagy by guiding the downstream pathways. Although interactions between p53 and eIF2α or eIF4E have been reported,[41,42] the exact mechanisms through which p53 mediates the modulation of p38 on eIF2α or eIF4E require further study.

In conclusion, we established a novel mechanistic link between the UPR and autophagy that may aid in developing new therapeutic modalities for malignant diseases. In addition, selenite exhibited significant antitumor effects *in vitro* and *in vivo*, suggesting its potential clinical application in leukemia therapy.

Materials and Methods

Cell culture and transfection. Human acute promyelocytic leukemia (APL)-derived NB4 cells were cultured in RPMI-1640 medium (Gibco BRL, Gaithersburg, MD, USA) supplemented with 10% FCS (TBD Science, Tianjin, China), 100 units/ml penicillin and 100 μg/ml streptomycin at 37°C in a 5% CO_2 humidified environment. The pCMV5-Flag-p38α (dominant negative) and pCMV-Neo-Bam p53 (R273H mutations) plasmids were purchased from Addgene (Cambridge, MA, USA). The pCMV-Hsp90 and pCMV-eIF4E plasmids were gifts from Professor YS (Institute of Basic Medicine, CAMS). The siRNAs directed against p38, PERK and eIF2α and a nonsilencing scrambled siRNA were synthesized by GenePharma (Shanghai, China) (see Supplementary Table S1 for the sequences). Cells were transfected with 5–10 μg of plasmids or 100–200 nM siRNA using Lipofectamine 2000 (Invitrogen, Carlsbad, CA, USA) or RNAiMAX (Invitrogen), respectively. Transfected cells were used for subsequent experiments after 24 h.

Xenograft model. Animal experiments were conducted according to the rules of the Institute of Hematology, Chinese Academy of Medical Sciences. Briefly, NB4 leukemia cells (5×10^6) were injected subcutaneously (s.c.) into the left flank of 4-week-old *nu/nu* mice. When tumors were visible, randomized cohorts were treated intraperitoneally with PBS or selenite (3 and 6 mg/kg) every other day for 3 consecutive weeks. Tumor diameters and body weights were measured up to three times weekly, and tumor volumes were calculated. For histologic analyses, tumor tissues were fixed in formalin, embedded in paraffin, sectioned and stained with hematoxylin and eosin (HE). For immunohistochemical inspection, tissue sections were stained with the indicated primary antibodies, incubated with secondary antibodies and then developed using a one-step horseradish peroxidase-labeled polymer method. Section observation and image collection were performed using a Zeiss KS400 image analysis system (Jena, Germany).

Reagents and antibodies. Sodium selenite, tunicamycin, 3-MA, Baf A1, anti-β-actin and anti-GST were purchased from Sigma-Aldrich (St. Louis, MO, USA). The chemical inhibitor 17-AAG (1 μmol/l) was purchased from Invivogen (San Diego, CA, USA). SB203580 (10 μM), salubrinal (5 μmol/l) and Mknk1 (1 μmol/l) were purchased from Calbiochem (San Diego, CA, USA). The anti-ATF4, anti-CHOP, anti-p-PERK, anti-p38, anti-MEK3/6 and anti-p-p53 antibodies were purchased from Santa Cruz Biotechnology (Santa Cruz, CA, USA). The anti-CD33 antibody was purchased from BIOSS (Beijing, China). All other antibodies were from Cell Signaling Technology (Danvers, MA, USA).

RNA extraction. Total RNA was extracted using the RNeasy mini kit (Qiagen, Gaithersburg, MD, USA) according to the manufacturer's instructions. Briefly, cells were centrifuged and washed, and the pellets were lysed with buffer RLT, transferred to RNeasy spin columns following the addition of ethanol, the RNeasy spin columns were washed and RNA was eluted. The eluted RNA was quantified using a NanoDrop ND-1000 UV-Vis Spectrophotometer (Thermo Scientific, Waltham, MA, USA). To test the integrity of the RNA, it was subjected to gel electrophoresis (Supplementary Figure S3).

qRT-PCR analysis. Reverse transcription was performed using M-MLV Reverse Transcriptase (Promega, Fitchburg, WI, USA). Then, synthesized cDNA was used for real-time PCR. Real-time PCR was performed using the SybrGreen PCR MasterMix and a 7500 real-time PCR system (Applied Biosystems, Carlsbad, CA, USA). Relative mRNA expression was determined by comparing the threshold cycle of amplified genes with that of GAPDH using the ΔCT method. Sequences for PCR primers are described in Supplementary Table S2.

Flow cytometric analysis of apoptosis. Annexin V-FITC apoptosis detection kit (Calbiochem) was used. Approximately 10^6 cells were harvested, washed twice with ice-cold PBS and stained with 1.25 μl of Annexin V-FITC in 0.5 ml of binding buffer for 15 min at room temperature. Then, binding buffer was replaced and cells were stained with PI. Apoptosis of cells was detected on Accuri C6 Flow Cytometer (BD Biosciences, Ann Arbor, MI, USA).

Growth inhibition assay. Cell growth was determined using the cell counting kit-8 (CCK-8) reagent (Dojindo, Mashikimachi, Japan). As instructed in the manual, cells were seeded in 96-well plates, stimulated with the indicated chemicals and then incubated with the CCK-8 reagent. Absorbance of each sample was measured with a Synergy H4 Hybrid Microplate Reader (BioTek, Winooski, VT, USA) at 450 nm with 620 nm as the reference wavelength.

Transmission electron microscopy. Cells were fixed in 2.5% glutaraldehyde for 1 h, post-fixed in 1% osmium tetroxide for 1 h at 48°C and then scraped and embedded in blocks of epon araldite. Ultrathin sections were stained with 4% aqueous uranyl acetate and lead citrate and examined with a JEOL (Akishima, Tokyo, Japan) TEM.

Extraction of cytoplasmic and nuclear fractions. Cells were harvested, washed and suspended in cytoplasmic extraction reagent (Boster Biological Technology, Wuhan, China) on ice for 30 min. Cells were pelleted at 12 000 × *g* for 10 min at 4°C, and supernatant was collected as the cytoplasmic fraction. Then, nuclear extraction reagent (Boster Biological Technology) was added, and the mixture was incubated on ice for 30 min, vortexed 10 s for 6 times and centrifuged at 12 000 × *g* for 10 min at 4°C. Supernatant was collected as the nuclear fraction.

Western blot analysis. Cells were lysed in RIPA buffer and subjected to sonication for 30 s. Cell lysates were centrifuged at 12 000 × *g* for 15 min at 4°C, and supernatant was collected. Protein concentrations were determined by Bradford assay. Then, equal amounts of proteins were fractionated onto 8 to 15% SDS-PAGE gels and transferred to nitrocellulose membranes. The membranes were blocked with 5% non-fat milk in TBST and probed with primary antibodies followed by horseradish peroxidase-labeled secondary antibodies. Blots were developed with SuperSignal West Pico Chemiluminescent Substrate

(Thermo Scientific). Then, the gray intensities of blots were measured using ImageJ software (Bethesda, MD, USA) and were normalized for β-actin or B23.

Co-immunoprecipitation. Cells were lysed and protein concentrations were adjusted to 2 μg/μl. Then, 2 μl of antibody was incubated with 100 μl of lysates overnight at 4°C. Next, 25 μl of protein A + G agarose beads (Santa Cruz Biotechnology) were added for 3 h at 4°C. Beads were washed three times, and bound proteins were eluted to subject to SDS-PAGE.

GST pull-down assays. Cell lysates were incubated overnight with 5 μg of GST-tagged p38 protein (Invitrogen) and then 30 μl of glutathione-agarose beads (Sigma-Aldrich) for 3 h at 4°C. After a thorough washing, bound proteins were eluted and subjected to a western blot assay.

Immunofluorescence. Cells were collected, fixed on glass slides and incubated with primary antibodies overnight at 4°C followed by FITC- or CY3-conjugated secondary antibody (Jackson ImmunoResearch Laboratories, West Grove, PA, USA) staining at room temperature for 1 h. Then, the cells were stained with 1 μmol/l DAPI (Sigma-Aldrich) for 5 min. Stained cells were observed under a fluorescence microscope (Carl Zeiss, Jena, Germany).

Chromatin immunoprecipitation assay. ChIP was performed using the SimpleChIP Enzymatic Chromatin IP Kit (Cell Signaling Technology) as previously described.[6] Briefly, proteins were crosslinked to DNA in living cells by adding formaldehyde (Sigma) to a final concentration of 1%. Then, the crosslinked cells were washed and swelled in Buffer A on ice for 10 min. After centrifugation, nuclei were pelleted and lysed with Buffer B. The resulting chromatin solution was digested and sonicated to generate DNA fragments. The supernatants were incubated with antibodies for 12–16 h at 4°C followed by immunoprecipitation with Protein G Agarose beads for 2 h at 4°C. After extensive washing, bound DNA fragments were eluted and subsequently analyzed by real-time PCR. Primers specific for the *MAP1LC3B* and *CHOP* promoters are listed in Supplementary Table S3.

***In situ* detection of DNA fragmentation.** The FragEL DNA Fragmentation Detection Kit (Calbiochem) was used to detect DNA strand breaks in xenograft tumors according to the manufacturer's instructions. Tissue slides were visualized using Zeiss Axioscope microscope.

Statistical analysis. The data shown are representative of at least three independent experiments and are presented as the means ± S.D. Statistical analysis was performed using ANOVA and Student's *t*-test. Results were considered significantly different at $P < 0.05$.

Conflict of Interest

The authors declare no conflict of interest.

Acknowledgements. We thank Dr. L Pan (China-Japan Friendship Hospital) for her expertise in immunocytochemistry assay. This work was supported by grants from the National Natural Sciences Foundation of China (No. 31170788 and No. 30970655), the National Natural Science Foundation for Young Scholars of China (No. 31101018), the Natural Science Foundation of Beijing (No. 5082015), the State Key Laboratory Special Fund (No. 2060204) and the Ministry of Education, China, for Doctor-training Unite (No. 20091106110025).

1. Licht JD. Acute promyelocytic leukemia–weapons of mass differentiation. *N Engl J Med* 2009; **360**: 928–930.
2. Salazar M, Hernandez-Tiedra S, Torres S, Lorente M, Guzman M, Velasco G. Detecting autophagy in response to ER stress signals in cancer. *Methods Enzymol* 2011; **489**: 297–317.
3. Hofius D, Munch D, Bressendorff S, Mundy J, Petersen M. Role of autophagy in disease resistance and hypersensitive response-associated cell death. *Cell Death Differ* 2011; **18**: 1257–1262.
4. Shi YH, Ding ZB, Zhou J, Hui B, Shi GM, Ke AW *et al.* Targeting autophagy enhances sorafenib lethality for hepatocellular carcinoma via ER stress-related apoptosis. *Autophagy* 2011; **7**: 1159–1172.
5. Shi K, Jiang Q, Li Z, Shan L, Li F, An J *et al.* Sodium selenite alters microtubule assembly and induces apoptosis in vitro and in vivo. *J Hematol Oncol* 2013; **6**: 7.
6. Jiang Q, Wang Y, Li T, Shi K, Li Z, Ma Y *et al.* Heat shock protein 90-mediated inactivation of nuclear factor-kappaB switches autophagy to apoptosis through becn1 transcriptional inhibition in selenite-induced NB4 cells. *Mol Biol Cell* 2011; **22**: 1167–1180.
7. Jiang Q, Li F, Shi K, Wu P, An J, Yang Y *et al.* ATF4 activation by the p38MAPK-eIF4E axis mediates apoptosis and autophagy induced by selenite in Jurkat cells. *FEBS Lett* 2013; **587**: 2420–2429.
8. Behrends C, Sowa ME, Gygi SP, Harper JW. Network organization of the human autophagy system. *Nature* 2010; **466**: 68–76.
9. Hayashi-Nishino M, Fujita N, Noda T, Yamaguchi A, Yoshimori T, Yamamoto A. A subdomain of the endoplasmic reticulum forms a cradle for autophagosome formation. *Nat Cell Biol* 2009; **11**: 1433–1437.
10. Rouschop KM, van den Beucken T, Dubois L, Niessen H, Bussink J, Savelkouls K *et al.* The unfolded protein response protects human tumor cells during hypoxia through regulation of the autophagy genes MAP1LC3B and ATG5. *J Clin Invest* 2010; **120**: 127–141.
11. Kroemer G, Marino G, Levine B. Autophagy and the integrated stress response. *Mol Cell* 2010; **40**: 280–293.
12. de la Cruz-Morcillo MA, Valero MLL, Callejas-Valera JL, Arias-González L, Melgar-Rojas P, Galán-Moya EM *et al.* P38MAPK is a major determinant of the balance between apoptosis and autophagy triggered by 5-fluorouracil: implication in resistance. *Oncogene* 2011; **31**: 1073–1085.
13. Kralova V, Benesova S, Cervinka M, Rudolf E. Selenite-induced apoptosis and autophagy in colon cancer cells. *Toxicol In Vitro* 2012; **26**: 258–268.
14. Zhan Y, Gong K, Chen C, Wang H, Li W. P38 MAP kinase functions as a switch in MS-275-induced reactive oxygen species-dependent autophagy and apoptosis in human colon cancer cells. *Free Radic Biol Med* 2012; **53**: 532–543.
15. Guan L, Han B, Li Z, Hua F, Huang F, Wei W *et al.* Sodium selenite induces apoptosis by ROS-mediated endoplasmic reticulum stress and mitochondrial dysfunction in human acute promyelocytic leukemia NB4 cells. *Apoptosis* 2009; **14**: 218–225.
16. Su J, Zhou L, Kong X, Yang X, Xiang X, Zhang Y *et al.* Endoplasmic reticulum is at the crossroads of autophagy, inflammation, and apoptosis signaling pathways and participates in the pathogenesis of diabetes mellitus. *J Diabetes Res* 2013; **2013**: 193461.
17. Heath-Engel HM, Chang NC, Shore GC. The endoplasmic reticulum in apoptosis and autophagy: role of the BCL-2 protein family. *Oncogene* 2008; **27**: 6419–6433.
18. Boyce M, Bryant KF, Jousse Cl, Long K, Harding HP, Scheuner D *et al.* A selective inhibitor of eIF2a protects cells from ER stress. *Science* 2005; **307**: 935–939.
19. Chang L, Karin M. Mammalian MAP kinase signalling cascades. *Nature* 2001; **410**: 37–40.
20. Ota A, Zhang J, Ping P, Han J, Wang Y. Specific regulation of noncanonical p38 activation by Hsp90-Cdc37 chaperone complex in cardiomyocyte. *Circ Res* 2010; **106**: 1404–1412.
21. Park MA, Curiel DT, Koumenis C, Graf M, Chen CS, Fisher PB *et al.* PERK-dependent regulation of HSP70 expression and the regulation of autophagy. *Autophagy* 2008; **4**: 364–367.
22. Rzymski T, Milani M, Pike L, Buffa F, Mellor H, Winchester L *et al.* Regulation of autophagy by ATF4 in response to severe hypoxia. *Oncogene* 2010; **29**: 4424–4435.
23. Koyanagi S, Hamdan AM, Horiguchi M, Kusunose N, Okamoto A, Matsunaga N *et al.* cAMP-response element (CRE)-mediated transcription by activating transcription factor-4 (ATF4) is essential for circadian expression of the Period2 gene. *J Biol Chem* 2011; **286**: 32416–32423.
24. Chen YJ, Tan BC, Cheng YY, Chen JS, Lee SC. Differential regulation of CHOP translation by phosphorylated eIF4E under stress conditions. *Nucleic Acids Res* 2010; **38**: 764–777.
25. Giovannini C, Vari R, Scazzocchio B, Sanchez M, Santangelo C, Filesi C *et al.* OxLDL induced p53-dependent apoptosis by activating p38MAPK and PKCdelta signaling pathways in J774A.1 macrophage cells. J. *Mol Cell Biol* 2011; **3**: 316–318.
26. Li Z, Shi K, Guan L, Cao T, Jiang Q, Yang Y *et al.* ROS leads to MnSOD upregulation through ERK2 translocation and p53 activation in selenite-induced apoptosis of NB4 cells. *FEBS Lett* 2010; **584**: 2291–2297.
27. Kelly LM, Yu JC, Boulton CL, Apatira M, Li J, Sullivan CM *et al.* CT53518, a novel selective FLT3 antagonist for the treatment of acute myelogenous leukemia (AML). *Cancer Cell* 2002; **1**: 421–432.
28. Kamimura T, Miyamoto T, Harada M, Akashi K. Advances in therapies for acute promyelocytic leukemia. *Cancer Sci* 2011; **102**: 1929–1937.
29. Kouroku Y, Fujita E, Tanida I, Ueno T, Isoai A, Kumagai H *et al.* ER stress (PERK/eIF2alpha phosphorylation) mediates the polyglutamine-induced LC3 conversion, an essential step for autophagy formation. *Cell Death Differ* 2007; **14**: 230–239.
30. Cherra SJ 3rd, Dagda RK, Chu CT. Review: autophagy and neurodegeneration: survival at a cost? *Neuropathol Appl Neurobiol* 2010; **36**: 125–132.
31. Keil E, Hocker R, Schuster M, Essmann F, Ueffing N, Hoffman B *et al.* Phosphorylation of Atg5 by the Gadd45beta-MEKK4-p38 pathway inhibits autophagy. *Cell Death Differ* 2013; **20**: 321–332.
32. Corcelle E, Djerbi N, Mari M, Nebout M, Fiorini C, Fenichel P *et al.* Control of the autophagy maturation step by the MAPK ERK and p38: lessons from environmental carcinogens. *Autophagy* 2007; **3**: 57–59.
33. Zheng YH, Tian C, Meng Y, Qin YW, Du YH, Du J *et al.* Osteopontin stimulates autophagy via integrin/CD44 and p38 MAPK signaling pathways in vascular smooth muscle cells. *J Cell Physiol* 2012; **227**: 127–135.
34. Park MA, Yacoub A, Rahmani M, Zhang G, Hart L, Hagan MP *et al.* OSU-03012 stimulates PKR-like endoplasmic reticulum-dependent increases in 70-kDa heat shock protein

expression, attenuating its lethal actions in transformed cells. *Mol Pharmacol* 2008; **73**: 1168–1184.
35. Manni S, Brancalion A, Tubi LQ, Colpo A, Pavan L, Cabrelle A *et al.* Protein kinase CK2 protects multiple myeloma cells from ER stress-induced apoptosis and from the cytotoxic effect of HSP90 inhibition through regulation of the unfolded protein response. *Clin Cancer Res* 2012; **18**: 1888–1900.
36. Al-Huseini LM, Aw Yeang HX, Sethu S, Alhumeed N, Hamdam JM, Tingle Y *et al.* Nuclear factor-erythroid 2 (NF-E2) p45-related factor-2 (Nrf2) modulates dendritic cell immune function through regulation of p38 MAPK-cAMP-responsive element binding protein/activating transcription factor 1 signaling. *J Biol Chem* 2013; **288**: 22281–22288.
37. Kumari G, Ulrich T, Gaubatz S. A role for p38 in transcriptional elongation of p21 (CIP1) in response to aurora B inhibition. *Cell Cycle* 2013; **12**: 2051–2060.
38. Crighton D, Wilkinson S, O'Prey J, Syed N, Smith P, Harrison PR *et al.* DRAM, a p53-induced modulator of autophagy, is critical for apoptosis. *Cell* 2006; **126**: 121–134.
39. Budanov AV, Karin M. p53 target genes sestrin1 and sestrin2 connect genotoxic stress and mTOR signaling. *Cell* 2008; **134**: 451–460.
40. Zhu N, Gu L, Findley HW, Zhou M. Transcriptional repression of the eukaryotic initiation factor 4E gene by wild type p53. *Biochem Biophys Res Commun* 2005; **335**: 1272–1279.
41. Yoon CH, Lee ES, Lim DS, Bae YS. PKR, a p53 target gene, plays a crucial role in the tumor-suppressor function of p53. *Proc Natl Acad Sci USA* 2009; **106**: 7852–7857.
42. Constantinou C, Elia A, Clemens MJ. Activation of p53 stimulates proteasome-dependent truncation of eIF4E-binding protein 1 (4E-BP1). *Biol Cell* 2008; **100**: 279–289.

Supplementary Information accompanies this paper on Cell Death and Disease website (http://www.nature.com/cddis)